Patient-derived malignant pleural mesothelioma cell cultures: A tool to advance biomarker-driven treatments

Nikolaos I. Kanellakis[1,2,3,4,*] , Rachelle Asciak[1,2,4,*], Megat Abd Hamid[5,6], Xuan Yao[5,6], Mark McCole[7], Simon McGowan[8], Elena Seraia[9], Stephanie Hatch[9], Eihab O. Bedawi[1,4], Rachel Mercer[1,4], Robert Hallifax[1,4], Stephanie Jones[10], Clare Verrill[10], Melissa Dobson[4], Vineeth George[1,4], Georgios T. Stathopoulos[11,12], Yanchun Peng[5,6], Daniel Ebner[9], Tao Dong[5,6], Najib M Rahman[1,2,3,4,**] and Ioannis Psallidas[1,2,4,**]

Affiliations:

1. Oxford Centre for Respiratory Medicine, Churchill Hospital, Oxford University Hospitals NHS Foundation Trust, Oxford, OX3 7LE, United Kingdom
2. Laboratory of Pleural and Lung Cancer Translational Research, Nuffield Department of Medicine, University of Oxford, Oxford, OX3 7FZ, United Kingdom
3. National Institute for Health Research Oxford Biomedical Research Centre, University of Oxford, Oxford, OX3 7LE, United Kingdom
4. Oxford Respiratory Trials Unit, Nuffield Department of Medicine, University of Oxford, Oxford, OX3 7LE, United Kingdom
5. Centre for Translational Immunology, Chinese Academy of Medical Sciences Oxford Institute, Nuffield Department of Medicine, University of Oxford, Oxford, OX3 7FZ, United Kingdom
6. Human Immunology Unit, MRC Weatherall Institute of Molecular Medicine, University of Oxford, Oxford, OX3 9DS United Kingdom
7. Cellular Pathology Department, John Radcliffe Hospital, Oxford University Hospitals NHS Foundation Trust, Oxford, OX3 9DU, United Kingdom
8. Computational Biology Research Group, MRC Weatherall Institute of Molecular Medicine, University of Oxford, Oxford, OX3 9DS United Kingdom

Kanellakis NI, *et al. Thorax* 2020; 75:1004–1008. doi: 10.1136/thoraxjnl-2020-215027

9. Cellular High Throughput Screening Facility, Target Discovery Institute, Nuffield Department of Medicine, University of Oxford, Oxford, OX3 7FZ, United Kingdom
10. Oxford Radcliffe Biobank, Nuffield Department of Surgical Sciences, John Radcliffe Hospital, University of Oxford, Oxford, OX3 9DU, United Kingdom
11. Molecular Lung Carcinogenesis Group, Comprehensive Pneumology Center and Institute for Lung Biology and Disease, Ludwig-Maximilians University and Helmholtz Center Munich, Bavaria, 81377, Germany
12. Laboratory for Molecular Respiratory Carcinogenesis, Department of Physiology, Faculty of Medicine; University of Patras; Rio, Achaia, 26504, Greece

* Equal co-authors

** Equal senior authors

Corresponding author:

Nikolaos I. Kanellakis

Laboratory of Pleural and Lung Cancer Translational Research, Nuffield Department of Medicine, University of Oxford, Oxford, OX3 7FZ, UK

Email: nikolaos.kanellakis@ndm.ox.ac.uk

Supplementary Methods

Study participants

Written informed consent was obtained from all participants prior to inclusion in the Oxford Radcliffe Pleural Biobank, reference number: 09/H0606/5+5 & 19/SC/0173, NHS Research Ethics Committee South Central Oxford C. All patients included in the study (March 2017 to February 2019) had pleural fluid and biopsies taken as part of their routine clinical care in the Oxford Pleural Unit. Data on progression and survival was derived from the clinical records.

MPM cell cultures establishment

Samples were collected from patients with MPM based on a histopathological (cytology/histology) or radiological diagnosis. At least 50 mls of the drained pleural fluid was sent for cytological examination in the local clinical cytology laboratory. Further pleural fluid specimens (approximately 50 mls) were processed by centrifugation (900g for 10 minutes) followed by red blood cell lysis (sterile filtered, 00-4333-57 Invitrogen, Waltham, MA). The cells were seeded in culture dishes (83.3902.300, Sarstedt, Nümbrecht, Germany). The time to generate a cell line varied between 30 to 60 days. Cells were observed daily using a ZEISS Primovert light microscope (Carl Zeiss AG, Oberkochen, Germany) and the growth of each sample was noted. Cancer cell colonies (Supplementary Figure 2) were observed in successfully established cell cultures. Cell culture medium was refreshed at least once a week for all cell cultures or more often based on the growth rate of the cells. Cells were passaged approximately at 80% confluency. Cell culture dishes were discarded and samples were marked as unsuccessful if a) cells were not adherent a

Kanellakis NI, *et al. Thorax* 2020; 75:1004–1008. doi: 10.1136/thoraxjnl-2020-215027

week after seeding or b) have not grown 60 days after seeding or c) became senescent after passaging.

Cell culture

All cells were cultured at 37 °C in 5% CO_2-95% air using DMEM (31966047 Gibco, Waltham, MA) supplemented with 10% FBS (10500-064 Gibco, Waltham, MA), 100 U ml^{-1} penicillin and 100 mg ml^{-1} streptomycin (P0781 Sigma -Aldrich, St. Louis, MO). For the experiments, cells were collected with trypsin (15090-046 Gibco, Waltham, MA) and counted with the TC20™ Automated Cell Counter (Bio-Rad, Hercules, CA). Cells were screened for *Mycoplasma Spp.* every four months (MP0035, Sigma -Aldrich, St. Louis, MO).

Cytology

Cytology specimens were prepared by cytocentrifugation (A78300003, ThermoFisher Scientific, Waltham, MA) at 500 G for 5 minutes. Cells were diluted in 0.1% w/v BSA/PBS (A9418 Sigma -Aldrich, St. Louis, MO). May Grunwald Giemsa staining was performed as previously described.. For each sample three cytological slides were made.

Tumour spheroids

Tumour spheres were generated as previously described.[1] In brief 5,000 cells per well were seeded using serum free medium in ultra-low attachment 96-well plates. Images were taken a week after seeding.

Molecular biology assays and gene expression

Cellular DNA and RNA were extracted and purified using the Blood & Cell Culture DNA Mini Kit (13323, Qiagen, Venlo, Netherlands) and RNeasy Plus Mini Kit (74134, Qiagen, Venlo, Netherlands) respectively as per instructions. For cDNA synthesis SuperScript IV (18091050 Invitrogen, Waltham, MA) was used. To measure gene expression qPCR was performed using specific primers (Supplementary Table 4, Sigma -Aldrich, St. Louis, MO) and LightCycler® 480 SYBR Green I Master (04707516001 Roche, Basel, Switzerland) in a LightCycler® 480 Instrument II cycler (05015243001 Roche, Basel, Switzerland) as per protocol. Ct values from triplicate reactions were analysed with the $2^{-\Delta\Delta CT}$ method as described elsewhere.[2]

Flow cytometry staining

Flow cytometry was conducted as previously described [3]. Data were acquired on an LSR Fortessa (Becton Dickinson BioSciences, Franklin Lakes, NJ) flow cytometer. Cells were stained with antibodies (Supplementary Table 5) as per protocol. Data were analysed on FlowJo version 10 software (Tree Star Inc., Ashland, OR).

Whole genome sequencing (WGS) and data analysis

WGS was conducted by Applied Biological Materials, Inc (Richmond, Canada) on an Illumina HiSeq X platform (Illumina, San Diego, CA). Pooled triplicate samples were used and starting material was 2 µg per sample. For the WGS analysis the GATK pipeline was used and BAM files were aligned to the GRCh38 human genome.[4] To identify somatic variants VarScan version 2.40 was used and the data filtered and visualised using MIG[5 6]. To evaluate the impact of the mutations that were present exclusively in late passage MPM cells logistic regression, radial support vector machine and ClinVar metrics were used as previously described. [7 8]

Kanellakis NI, *et al. Thorax* 2020; 75:1004–1008. doi: 10.1136/thoraxjnl-2020-215027

High throughput drug screening

High throughput drug screening was performed in collaboration with the Cellular High Throughput Screening facility at the Target Discovery Institute, Nuffield Department of Medicine, University of Oxford, United Kingdom. A drug library (TDI Expanded Oncology Drug Set, Supplementary Table 3) of 316 agents was used. Cells were seeded in 384 well plates (3712, Corning, Corning, NY) using a JANUS® G3 automated liquid handling workstation (AJV001, Perkin Elmer, Waltham, MA) at 2,000 cells per well for MESO-163 and 1,600 cells per well for MESO-174 and MESO-031. The number of cells to be seeded was chosen based on the growth dynamics of each cell culture. Three different concentrations of the drugs were tested in duplicate: 100 nM, 1 μM and 10 μM. The compounds were dispensed with an Echo 550 liquid handler (Labcyte, San Jose, CA) and then diluted using the JANUS workstation. Drugs were added to the culture media 24 hours post seeding the cells. Cellular viability was measured 48 hours post treatment with the resazurin assay. The media was changed to phenol red-free DMEM media (31053-028, Gibco, Waltham, MA) containing 10% FBS and 10ug/ml resazurin (199303, Sigma-Aldrich, St. Louis, MO) and 2 hours later, fluorescence was measured with an EnVision 2104 Multilabel Reader (Perkin Elmer, Waltham, MA).

To perform the clustering analysis the pheatmap function from the pheatmap (v 1.0.12) R package (v 3.5.3) and the Pearson correlation as metric were used.

MPM and T cell co-culture assays

The cancer-specific T cells were provided by Prof. Tao Dong. Intra-cellular cytokine staining (ICS) and cytotoxic T cell killing assay were performed in triplicates as

Kanellakis NI, *et al. Thorax* 2020; 75:1004–1008. doi: 10.1136/thoraxjnl-2020-215027

described elsewhere [3]. In brief, MPM cancer cells were peptide-loaded with an $SSX2^{41-49}$-specific KV9 peptide (KASEKIFYV). For the peptide-loading three different peptide concentrations were used: 2 μM, 0.8 μM, 0.04 μM. No peptide-loaded (0 μM) MPM cells were used as a negative control. For the ICS, T cells were treated with Monensin (554724, Becton Dickinson BioSciences, Franklin Lakes, NJ) and Brefeldin A (555029, Becton Dickinson BioSciences, Franklin Lakes, NJ) before co-cultured with the stimulated and control MPM cells for 5 hours at 37 ^{o}C. Cell fixation was done with Fixation/Permeabilization Solution Kit (554714, Becton Dickinson BioSciences, Franklin Lakes, NJ) followed by antibody staining (Supplementary Table 3). For the cytotoxic T cell killing assay, MPM cells were stained with CFSE (C34554 Invitrogen Scientific, Waltham, MA) before peptide-loaded and later co-cultured with the cancer-specific T cells for 5 hours at 37 ^{o}C. Subsequently, cells were stained with 7-AAD (00-6993-50 Invitrogen Scientific, Waltham, MA). MPM cell viability was measured by the $CFSE^{+}7AAD^{-}$ population, using an Attune NxT flow cytometer (ThermoFisher, Scientific, Waltham, MA).

Microscopy

Live cell microscopy images were taken using a ZEISS Axio Observer (Carl Zeiss AG, Oberkochen, Germany) microscope. Pleural fluid cytology and pleural biopsy histology images were taken using an Olympus BX43 (Olympus, Tokyo, Japan).

Availability of data

Whole genome sequencing data are available at Sequence Read Archive (SRA) database of National Center for Biotechnology Information (NCBI). Submission reference: SUB6545415.

Statistics

Statistical analyses were conducted using Prism v8.0 (GraphPad, La Jolla, CA). Values are given as mean±SEM. Comparisons were conducted by one- or two-way ANOVA with Tukey's multiple comparison correction. P values $P < 0.05$ was considered significant.

Kanellakis NI, *et al. Thorax* 2020; 75:1004–1008. doi: 10.1136/thoraxjnl-2020-215027

Supplementary Figures

Supplementry Figure 1. Cytological and histological examination of malignant pleural effusion and pleural biopsy specimens confirmed their malignant nature.

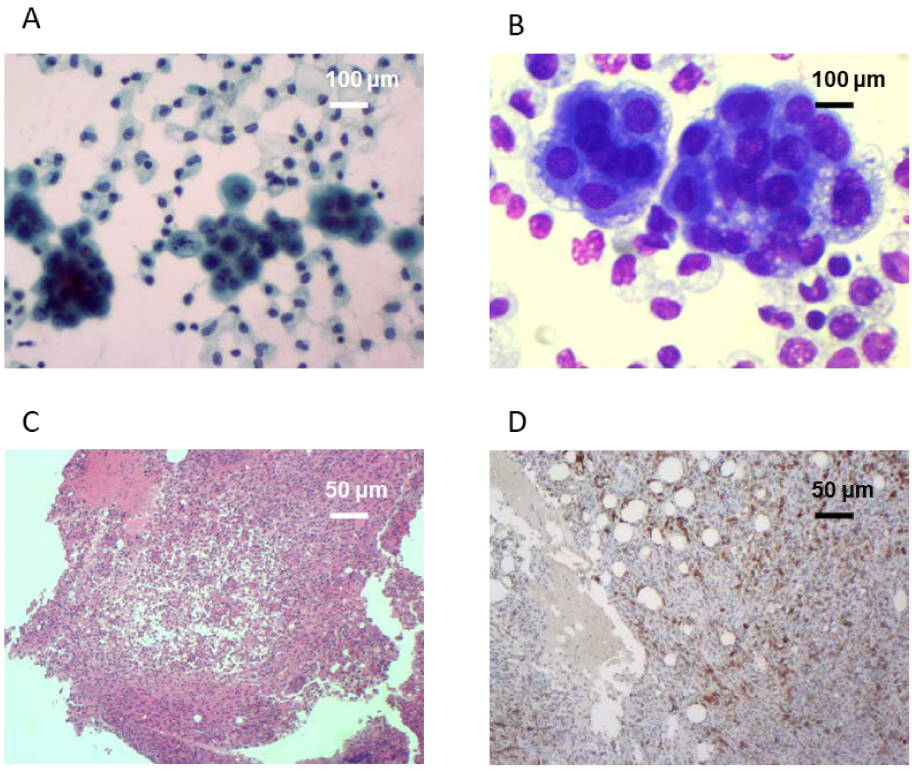

Malignant pleural effusion and pleural biopsy specimens were sent for cytological and histological examination. **(A)** Papanicolaou stained pleural fluid cytology speciment (10X magnification). There are atypical cells arranged in small papillaroid clusters. These cells have mesothelial morphology. **(B)** May Grunwald Giemsa stained pleural fluid cytology speciment (10X magnification). The appearances of the cells are those of an atypical mesothelial proliferation suspicious of mesothelioma. **(C)** Hematoxylin and Eosin stained pleural biopsy (5X magnification). Histology shows pattern of solid growth epithelioid malignant mesothelioma. **(D)** Cytokeratin 5

Kanellakis NI, *et al. Thorax* 2020; 75:1004–1008. doi: 10.1136/thoraxjnl-2020-215027

immunohistochemistry stained pleural biopsy (5X magnification). Pleural tissue has been widely infiltrated by a biphasic malignant mesothelioma with a compatible immunophenotype (CK5 positive). There is also necrosis and invasion of the pleural fat. Stainiings were done as per standard National Health Service (NHS) protocols.

Kanellakis NI, *et al. Thorax* 2020; 75:1004–1008. doi: 10.1136/thoraxjnl-2020-215027

Supplementry Figure 2. Live cell imaging shows MPM cells growing in colonies.

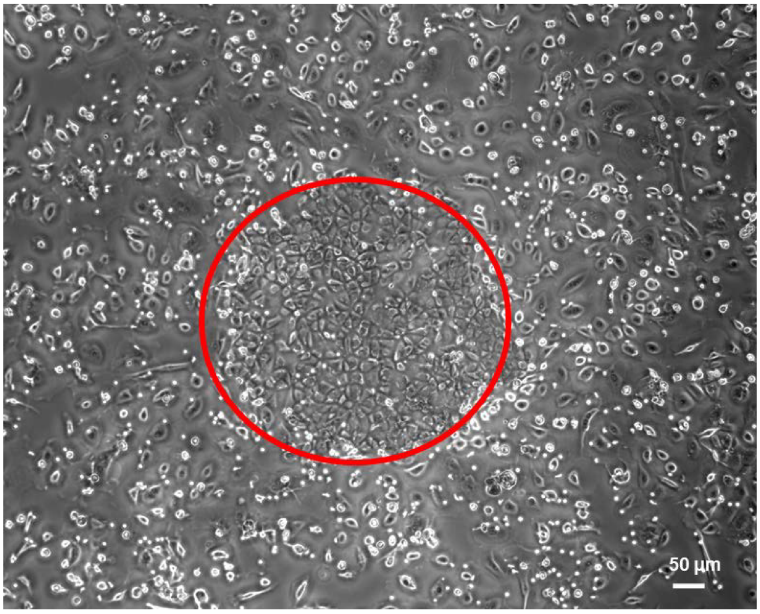

A cancer cell colony (in the red circle), growing surrounded by other mixed cells (5X magnification). Note the differences between the cancer and mixed cells. This image was taken five days post seeding the malignant pleural effusion cells.

Kanellakis NI, *et al. Thorax* 2020; 75:1004–1008. doi: 10.1136/thoraxjnl-2020-215027

Supplementry Figure 3. The mutations detected by the whole genome sequencing analysis were predominately heterozygous.

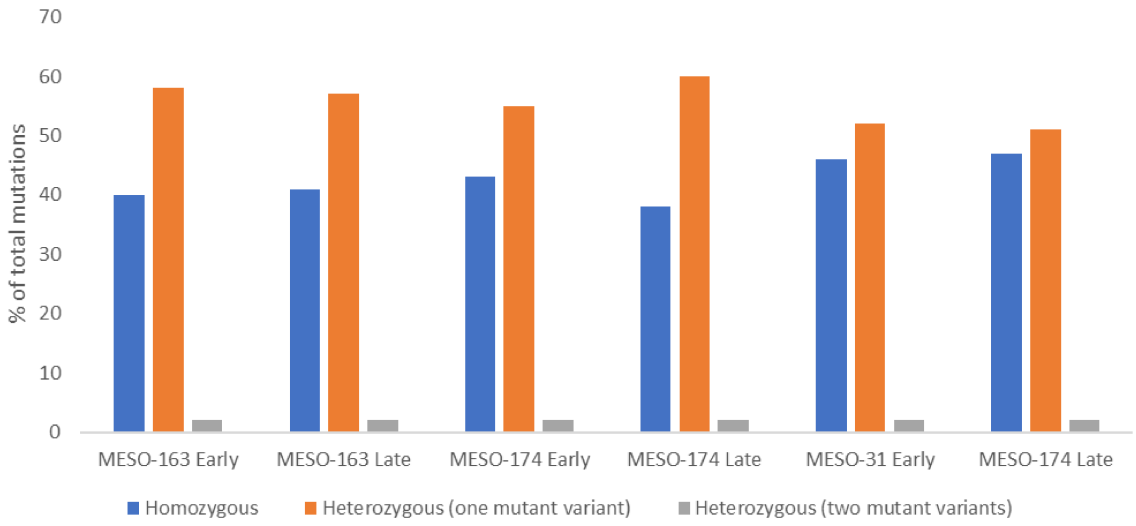

The whole genome sequencing analysis revealed that in the majority the detected mutations were heterozygous with one mutant variant (55% in average), followed by homozygous (43%) and heterozygous where both variants were mutant (2%).

Kanellakis NI, *et al. Thorax* 2020; 75:1004–1008. doi: 10.1136/thoraxjnl-2020-215027

Supplementry Figure 4. The synonymous and non-synonymous mutation rates.

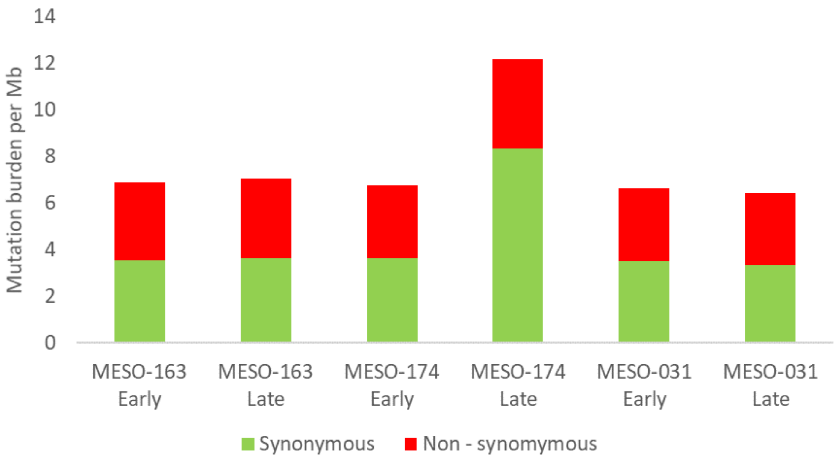

Barplots showing the synonymous and non-synonymous mutation rates per Mb for the sequenced patient-derived MPM cell cultures at two timepoints (early – Passage 0 and late – Passage 20). With the exception of MESO-174 (biphasic MPM) that exhibited increased burden of synonymous mutations at the late passage (~8 mutations per Mb), the other cell cultures displayed similar rates (~3 mutations per Mb) of synonymous and non-synonymous mutations.

Supplementry Figure 5. The percetange of transitions and transversions

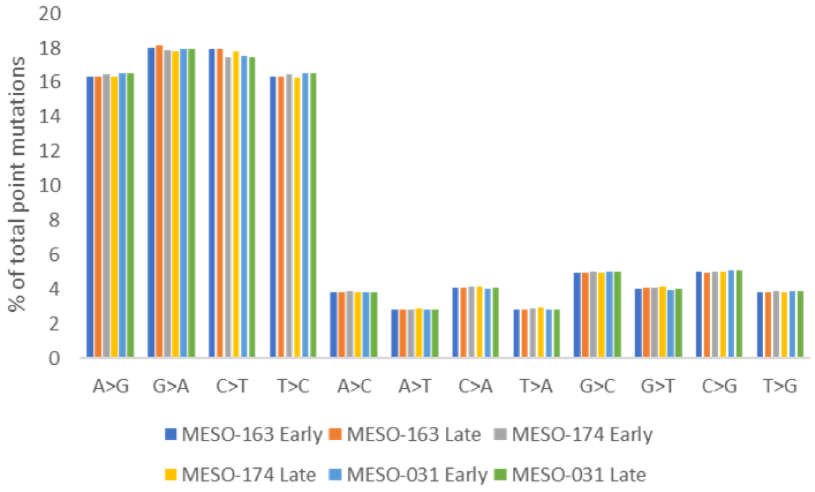

Barplots showing the frequency of transitions (A>G, G>A, C>T, T>C) and transversions (A>C, A>T, C>A, T>A, G>C, G>T, C>G, T>G). The point mutations were predominately transitions with a rate of 68%.

Supplementry Figure 6. Agreement between the high-throughout drug screening replicates.

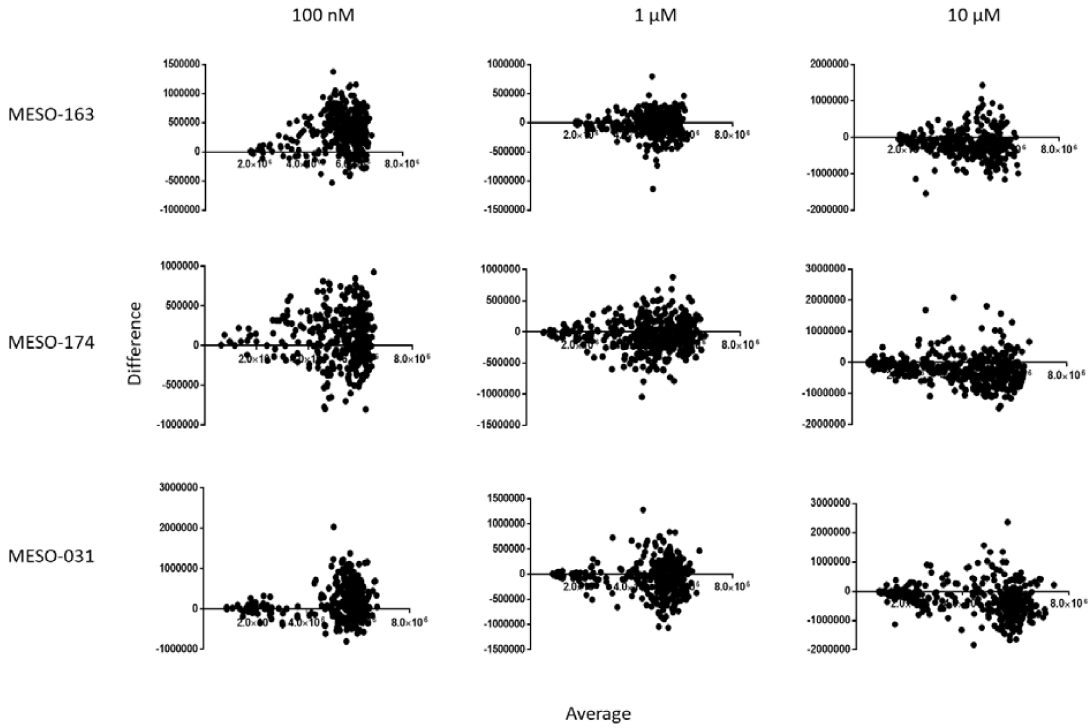

Bland - Altman plots showing the agreement between two replicates of the high-throughput drug screening assay.

Supplementry Figure 7. The high-throuput drug screening assay revealed anticancer agents that were *in vitro* more efficient compared to pemetrexed cisplatin.

Anticancer agent	MPM cell line									Target
	MESO-163			MESO-031			MESO-174			
	100nm	1um	10um	100nm	1um	10um	100nm	1um	10um	
Cisplatin / Pemetrexed	**-3.3**	**-2.4**	**-1.4**	**-2.4**	**-1.7**	**-0.9**	**-0.9**	**-0.5**	**0.2**	
Bortezomib	-3.8	-2.8	-1.7	-3.7	-2.8	-1.7	-2.7	-2.2	-1.4	Proteasome inhibitor
Dinaciclib (SCH727965)	-3.7	-2.6	-1.6	-3.0	-2.1	-1.2	-3.0	-2.0	-1.2	CDK inhibitor
Idarubicin HCl	-3.7	-2.8	-1.8	-3.2	-2.6	-1.6	-3.5	-2.4	-1.7	Topoisomerase II inhibitor
Omacetaxine mepesuccinate	-3.4	-2.8	-1.7	-3.3	-2.7	-1.6	-3.2	-2.4	-1.6	Protein synthesis inhibitor
Dactinomycin	-3.7	-2.8	-1.7	-3.2	-2.5	-1.4	-2.9	-2.2	-1.3	RNA and DNA synthesis inhibitor
Carfilzomib	-3.7	-2.7	-1.7	-3.7	-2.7	-1.7	-3.5	-2.4	-1.6	Proteasome inhibitor
Romidepsin	**-3.0**	**-2.2**	-1.6	-3.5	-2.6	-1.7	-3.8	-2.6	-1.7	HDAC inhibitor
Panobinostat	**-2.1**	-1.8	-1.2	-3.1	-2.5	-1.6	-3.7	-2.6	-1.7	HDAC inhibitor
Gemcitabine hydrochloride	-1.4	-0.9	-0.2	-3.1	-2.5	-1.5	-1.7	-1.6	-1.0	Nucleoside analog
Paclitaxel	-1.8	-1.2	0.0	-3.0	-2.2	-1.1	-2.1	-1.5	-0.5	Microtubule stabilizer
Vinblastine sulfate	**-2.5**	-1.7	-0.9	-3.0	-2.2	-1.4	-2.9	-2.2	-1.5	Mitotic inhibitor. Vinca alkaloid microtubule depolymerizer
Daunorubicin hydrochloride	**-2.4**	**-2.8**	-1.7	-2.9	-2.7	-1.6	-2.9	-2.3	-1.6	Topoisomerase II inhibitor
Docetaxel	-1.7	-1.3	-0.2	-2.9	-2.1	-1.1	-2.2	-1.5	-0.5	Microtubule stabilizer
KX2-391	**-2.2**	-1.5	-0.8	-2.9	-2.1	-1.2	-1.8	-1.7	-1.1	SRC inhibitor
Ixabepilone	-1.2	-1.4	-0.7	-2.8	-2.1	-1.2	-1.9	-1.4	-0.6	Mitotic inhibitor. Epothilone microtubule stabilizing
Cabazitaxel	-1.3	-0.5	0.1	-2.8	-1.9	-1.0	-2.0	-1.1	-0.1	Taxane microtubule stabilizer
Mitoxantrone	**-2.6**	**-2.7**	-1.7	-2.8	-2.6	-1.6	-3.2	-2.5	-1.7	Topoisomerase II inhibitor
Epothilone B (Patupilone)	-1.8	-0.6	0.0	-2.7	-2.0	-1.1	-2.2	-1.1	0.0	Microtubule stabilizing
Vinorelbine tartrate	**-2.2**	-1.8	-1.0	-2.7	-2.2	-1.3	-2.1	-1.8	-1.3	Mitotic inhibitor. Vinca alkaloid microtubule depolymerizer
BI 6727_Volasertib	**-2.3**	-1.3	-1.5	-2.5	-2.1	-1.2	-1.4	-0.8	-0.7	PLK1 inhibitor
JNJ-26481585_Quisinostat	**-2.2**	-1.9	-1.3	-2.5	-2.5	-1.6	-3.4	-2.6	-1.7	HDAC inhibitor
UCN-01	-0.7	-0.4	-1.7	-1.4	-1.7	-1.5	-2.7	-2.1	-1.7	PDK1 inhibitor
INK128	-2.0	-2.0	-1.2	-0.3	-0.7	-0.6	-2.4	-1.7	-1.0	mTOR inhibitor
Plicamycin	-2.9	-2.8	-1.7	-1.9	-2.2	-1.4	-2.3	-2.1	-1.1	RNA synthesis inhibitor
Topotecan hydrochloride	-1.4	-1.6	-1.5	-2.3	-2.6	-1.0	-2.1	-1.9	-1.3	Topoisomerase I inhibitor
Camptothecin	-1.4	-1.6	-1.5	-2.3	-2.6	-1.2	-1.9	-2.1	-1.2	Topoisomerase I inhibitor
Mithramycin A	-2.5	-2.8	-1.7	-1.4	-2.2	-1.4	-1.9	-2.1	-1.1	RNA synthesis inhibitor
17-AAG (Tanespimycin, Geldanamycin)	-0.9	-0.9	-0.7	-1.4	-1.8	-1.0	-1.8	-1.4	-0.5	HSP90 inhibitor
Doxorubicin	-1.1	-2.4	-1.7	-1.9	-2.5	-1.5	-1.8	-2.4	-1.4	Topoisomerase II inhibitor
NVP-AUY922	-1.8	-1.1	-0.5	-2.2	-1.7	-1.0	-1.8	-1.1	-0.5	HSP90 inhibitor
17-DMAG (Alvespimycin)	-1.4	-1.3	-1.4	-1.9	-1.5	-1.0	-1.7	-1.1	-1.5	HSP90 inhibitor
Epirubicin hydrochloride	-1.0	-2.3	-1.7	-1.8	-2.5	-1.6	-1.7	-2.4	-1.5	Topoisomerase II inhibitor
GSK2126458	-1.5	-1.8	-1.1	-1.0	-1.3	-0.7	-1.6	-1.8	-1.0	P110α/β/δ/γ and mTORC1/2 inhibitor
R406_Tamatinib	-1.8	-1.7	-0.9	-0.1	-1.8	-1.1	-1.5	-1.8	-0.9	SYK inhibitor
AZD8055	-1.0	-1.6	-1.0	-0.2	-1.1	-0.5	-1.5	-2.0	-1.1	mTOR inhibitor
SB 743921	-2.1	-1.4	-1.7	-2.3	-1.6	-1.7	-1.5	-0.8	-1.7	Mitotic inhibitor. KSP inhibitor
TAK-901	-1.5	-2.2	-1.7	-0.6	-1.7	-1.4	-1.3	-2.5	-1.6	Aurora inhibitor
Ixazomib citrate	-1.6	-2.7	-1.7	0.1	-2.7	-1.7	-1.3	-1.7	-1.1	Proteasome inhibitor
RAF265	-0.1	0.0	-0.2	0.4	0.5	0.0	-1.2	-0.9	-0.2	C-Raf/B-Raf/B-Raf (V600E) and VEGFR2 phosphorylation inhibitor
Dasatinib	-1.1	-0.4	-0.1	-0.5	-0.8	-0.3	-1.0	-0.9	-0.6	ABL, SRC and c-KIT inhibitor
MK1775	0.0	-1.0	-0.8	0.3	-0.2	-1.1	-1.0	-1.0	-0.5	WEE1 inhibitor
AP24534 (Ponatinib)	-1.9	-2.4	-1.7	-0.3	-0.6	-1.7	-1.0	-1.5	-1.7	ABL, PDGFRα, VEGFR2, FGFR1 and SRC inhibitor
PIK-75 HCl	0.0	-2.4	-1.7	0.6	-2.0	-1.5	-1.0	-1.8	-1.2	P110α inhibitor
Rapamycin (sirolimus)	-1.0	-0.5	0.1	-0.1	-0.3	0.4	-1.0	-0.9	0.1	mTOR inhibitor

The Z factor metric is used to describe the separation between the negative and positive controls in high throughput assays. In our drug screen the average Z factor for the MESO-163 and MESO-031 cell cultures, was 0.6 and 0.5 respectively, indicating a good assay window between the negative control (0.1% DMSO) and the positive control (10uM/1.6uM pemetrexed/cisplatin). On the other hand, the Z factor

was less than zero for MESO-174, indicating little difference in its' response to the positive and negative controls.

The figure presents the anticancer agents that had a lower z-score compared to pemetrexed/cisplatin (positive control, on top) and thus were more efficient. Drugs in salmon background (in total six) were more efficient for all MPM cells, in mustard (in total 21) for MESO-031 and MESO-174 (in total 44) and in blue only for MESO-174.

Kanellakis NI, *et al. Thorax* 2020; 75:1004–1008. doi: 10.1136/thoraxjnl-2020-215027

Supplementary Figure 8. Flow cytometry analysis detected four MPM cell cultures HLA-A2^{+}.

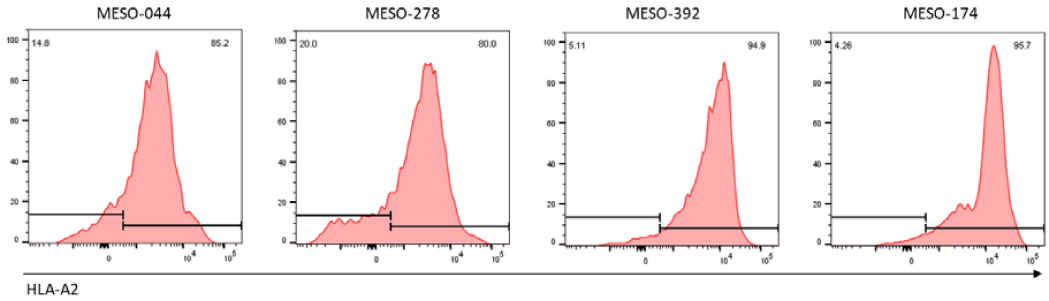

Prior performing the co-culture assays we screened the MPM cells for HLA-A2 expression as the cancer specific T cells were HLA-A2 restricted. We identified four cell cultures that were HLA-A2^{+}, which were used for the co-culture experiments. The figure presents the frequency histograms of HLA-A2 expression for the four cell cultures.

Supplementary Figure 9. FACS contour plots showing CD107a⁺ CD8⁺ T cells.

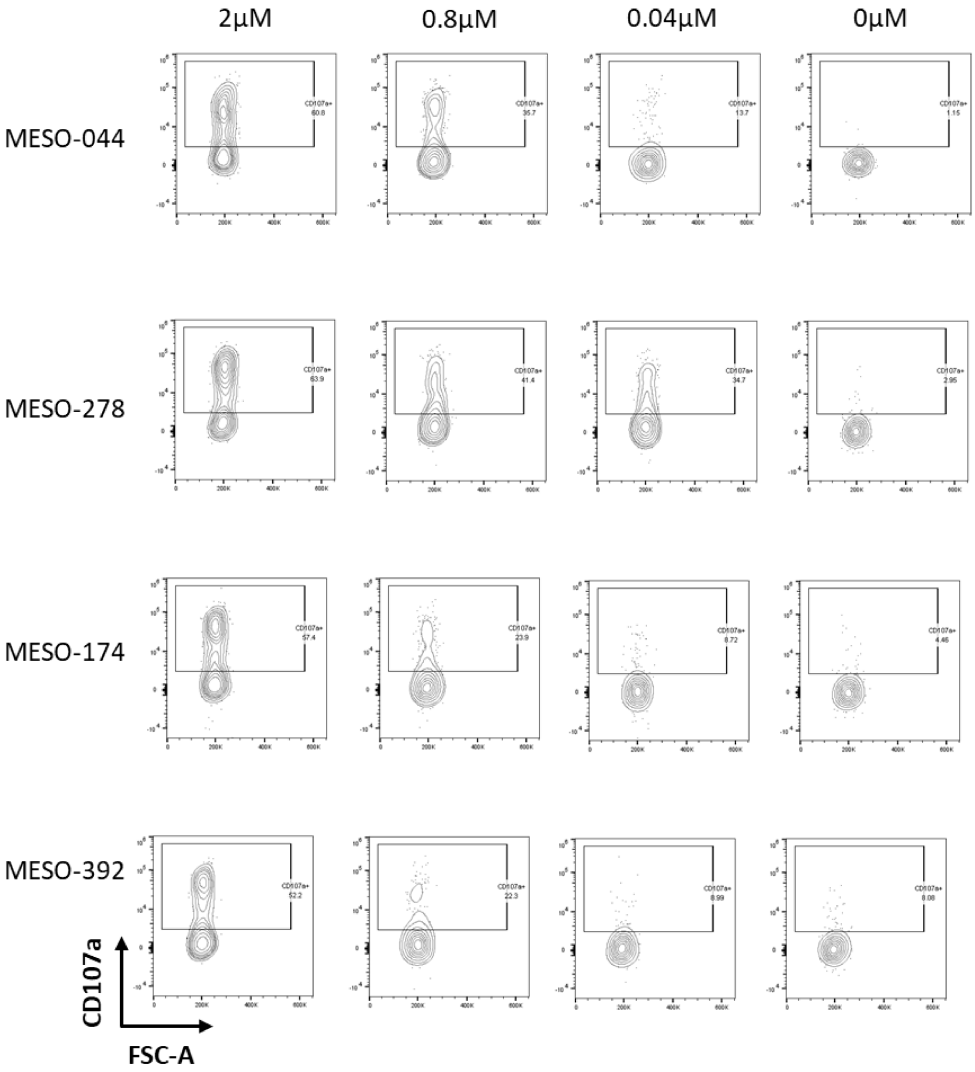

FACS contour plots of CD107a staining of CD8⁺ T cells upon co-culture with selected MPM cell cultures (epithelioid: MESO-044, MESO-278 and biphasic: MESO-174, MESO-392) which were SSX2-peptide loaded (from left: 2µM, 0.8µM, 0.04µM) and control (0µM). Interestingly the biphasic cell cultures triggered T cell degranulation even without peptide loading. Triplicate samples were used per cell culture/condition.

Supplementary Figure 10. FACS dot plots showing the IFNγ⁺ and TNFa⁺ CD8⁺ T cells.

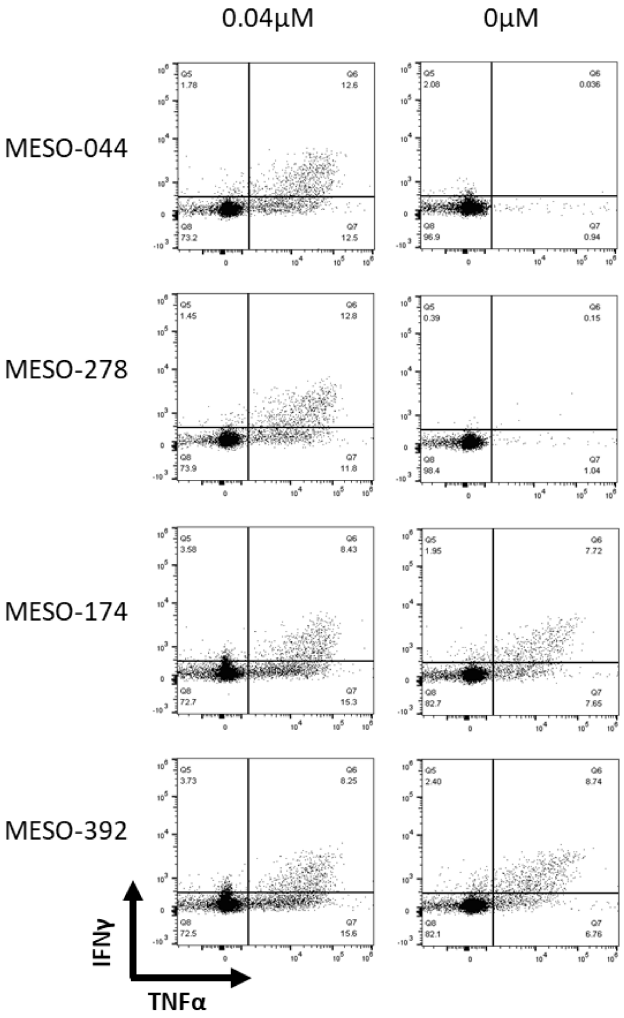

FACS dot plots representing the CD8⁺ T cell expression of IFNγ and TNFα cytokines, upon co-culture with SSX2 pulsed (0.04μM) and control (no pulse) MPM cells (epithelioid: MESO-044, MESO-278 and biphasic: MESO-174, MESO-392). The co-culture with the non-SSX2 pulsed biphasic MPM cells (control group) induced the production of T cell IFNγ and TNFα. Triplicate samples were used per cell culture/condition.

Supplementary Figure 11. Co-culture of cancer-specific CD8+ T cells with SSX2-peptide loaded MPM cells at varying peptide concentrations triggered the induction of the degranulation factor CD107a.

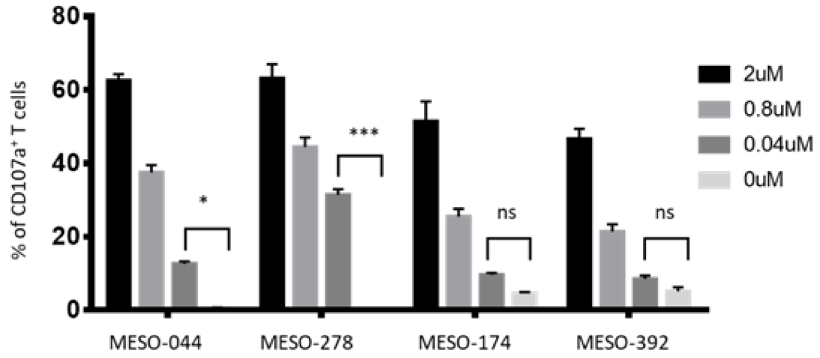

Tukey's multiple comparisons test for 0uM vs 0.04 uM	Mean Diff.	95% CI of diff.	Adjusted P Value
MESO-044 vs MESO-278	0	-2.082 to 2.082	> 0.9999
MESO-044 vs MESO-174	-13.12	-15.20 to -11.03	< 0.0001
MESO-044 vs MESO-392	-14.63	-16.71 to -12.54	< 0.0001
MESO-278 vs MESO-174	-13.12	-15.20 to -11.03	< 0.0001
MESO-278 vs MESO-392	-14.63	-16.71 to -12.54	< 0.0001
MESO-174 vs MESO-392	-1.51	-3.592 to 0.5722	0.1718

Barplot presenting the percentage of CD107a+ T cells upon co-culture with selected MPM cells (epithelioid: MESO-044, MESO-278 and biphasic: MESO-174, MESO-392) which were SSX2-peptide loaded. Note that the biphasic cell cultures triggered production of CD107a even without the SSX2-peptide loading. ***, * and ns denote $P< 0.001$, $P<0.05$ and not significant respectively, for comparisons by two-way ANOVA with Tukey's post-tests. Data are summarised as mean ± SEM. Triplicate samples were used per cell culture/condition.

Supplementary Figure 12. Co-culture of cancer-specific CD8+ T cells with SSX2-peptide loaded MPM cells at varying peptide induced T cell killing capacity.

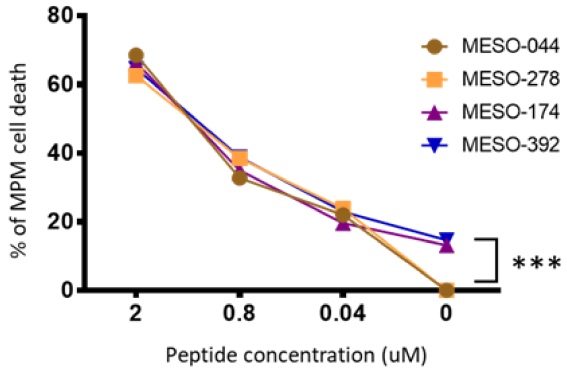

MPM Cell Culture 1 0uM	MPM Cell Culture 2 0uM	Mean Diff.	95.00% CI of diff.	Adjusted P Value
MESO-044	MESO-278	0	-7.205 to 7.205	>0.9999
MESO-044	MESO-174	-13.12	-20.32 to -5.912	<0.0001
MESO-044	MESO-392	-14.63	-21.83 to -7.422	<0.0001
MESO-278	MESO-174	-13.12	-20.32 to -5.912	<0.0001
MESO-278	MESO-392	-14.63	-21.83 to -7.422	<0.0001
MESO-174	MESO-392	-1.51	-8.715 to 5.695	>0.9999

Graph presenting the killing capacity of the T cells upon co-culture with the SSX2-peptide loaded MPM cells (epithelioid: MESO-044, MESO-278 and biphasic: MESO-174, MESO-392). The vertical axis shows the percentage of MPM cell death and the horizontal the SSX2 peptide concentration. Notably the biphasic MPM cells triggered T cells cytotoxicity even without the peptide loading. A statistically significant difference was detected at 0 μM between each of the biphasic and each of the epithelioid cell cultures (MESO174 vs MESO-044/MESO-278, MESO-392 vs MESO044/MESO278). The T cell cytotoxicity for the highest concentration of the peptide loading confirms the effectiveness of the CD8+ T cells (positive control). ***

denote < 0.001, for comparisons by two-way ANOVA with Tukey's post-tests. Data are summarised as mean ± SEM. Triplicate samples were used per cell culture/condition

Kanellakis NI, *et al. Thorax* 2020; 75:1004–1008. doi: 10.1136/thoraxjnl-2020-215027

Supplementary Figure 13. Co-culture of cancer-specific CD8+ T cells with SSX2-peptide loaded MPM cells at varying peptide concentrations triggered the expression of the cytotoxic factors INFγ and TNFa.

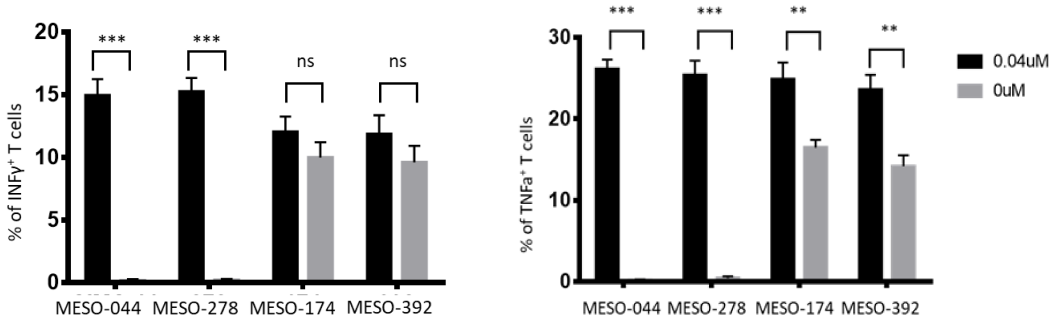

Tukey's multiple comparisons test for 0uM vs 0.04 uM	Mean Diff.	95.00% CI of diff.	Adjusted P Value
MESO-044	14.76	9.556 to 19.96	<0.0001
MESO-278	15.04	9.833 to 20.24	<0.0001
MESO-174	2.053	-3.149 to 7.254	0.8874
MESO-392	2.258	-2.944 to 7.459	0.8311

Tukey's multiple comparisons test for 0uM vs 0.04 uM	Mean Diff.	95.00% CI of diff.	Adjusted P Value
MESO-044	25.91	19.56 to 32.27	<0.0001
MESO-278	24.93	18.57 to 31.28	<0.0001
MESO-174	8.365	2.009 to 14.72	0.0045
MESO-392	9.413	3.056 to 15.77	0.0012

Barplots of IFNγ (left) and TNFα (right) expression by the T cells upon co-culture with SSX2-peptide loaded (0.04μM) and control (no pulse) MPM cells (epithelioid: MESO-044, MESO-278 and biphasic: MESO-174, MESO-392). The biphasic MPM cell cultures induced the IFNγ and TNFα cytokine expression of T cells even without the peptide loading. *** and ns denote $P < 0.001$ and not significant respectively, for comparisons by two-way ANOVA with Bonferroni post-tests. Data are summarised as mean ± SEM. Triplicate samples were used per cell culture/condition.

Supplementary Tables

Supplementary Table 1. Patient demographic characteristics.

	Cell culture successfully generated cohort n=16		Cell culture unsuccessfully generated cohort n=20	
	Range	Median (IQR) / N	Range	Median (IQR) / N
Gender	NA	F=2, M=14	NA	F=4, M=16
Age (years)	56, 87	78 [67, 83]	64, 92	77 [69, 83]
MPM Subtype	NA	Epithelioid: 13 Biphasic: 3	NA	Epithelioid: 16 Biphasic: 4
Cytology of drained malignant pleural effusion	NA	Positive/suspicious: 15 Negative: 1	NA	Positive/suspicious: 12 Negative: 6 Mis=2
Haemoglobin g/dL	11.10, 16.60	14.10, [13.70, 15.10]	9.50, 17.40	13.65 [12.43, 15.23
Urea mg/dL	2.60, 13.40	4.90 [3.90, 10.0]	2.40, 26.20	5.65 [4.07, 9.82]
White cells counts 10^9/L	4.30, 14.20	8.90 [5.80, 11.30]	3.90, 14.10	8.45 [6.12, 10.70]
Platelet 10^9/L	109.00, 411.00	265.00 [246.00, 315.00]	194.00, 789.00	293.50 [233, 382]
Albumin g/dL	27.00, 40.00	34.00 [31.00, 37.00]	23.00, 47.00	31.50 [27.25, 36.00]
Glucose pleural fluid mmol/L	1.50, 9.60	5.00 [2.48, 6.23]	0.60, 6.10	4.25 [2.70, 5.25]
LDH pleural fluid IU/L	88.00, 1934.00	221.00 [154.3, 673.50]	95, 8015	319.50 [162.30, 815.80]
Protein pleural fluid mg/ml	36.00, 52.00	40.00 [38.25, 45.75]	31.00, 54.00	44.50 [37.75, 50.25]

IQR = interquartile range, N = sample size, NA = Not Applicable, MPM = Malignant Pleural Mesothelioma, Mis = Missing data

Sixteen MPM cell cultures were established from a total of 36 MPM pleural effusion samples (success rate of 45%). The panel of MPM cell cultures was derived from a predominately male (88%) and histologically epithelioid (81%) cohort with a median age of 78 years. The time to generate an MPM cell culture varied greatly among the samples with an average of two months. Of the sixteen generated MPM cell cultures, pleural fluid cytology analysis reported features consistent with MPM for the majority (15/16, 94%), while one cell culture (1/16, 6%) was derived from a negative cytology

pleural fluid. We were able to successfully establish cell cultures from patients at several different drainage timepoints. Each cell culture was clonogenic, and able to recover and regrow following cryopreservation and thawing

Kanellakis NI, *et al. Thorax* 2020; 75:1004–1008. doi: 10.1136/thoraxjnl-2020-215027

Supplementary Table 2. Mutations present exclusively at the late passage that are predicted to be pathogenic.

MPM cell culture	Chromosome	Gene	Radial SVM score	Radial SVM pred	LR score	LR pred	CLNSIG	CLNREVSTAT
MESO-031	3	MLH1	-0.647	T	0.293	T	Pathogenic	Reviewed by expert panel
	20	GNAS	0.786	D	0.831	D	NA	NA
MESO-174	3	GATA2	0.525	D	0.853	D	NA	NA
	3	GATA2	0.504	D	0.84	D	NA	NA
	3	GATA2	0.06	D	0.771	D	NA	NA
	3	GATA2	-0.27	T	0.676	D	NA	NA
	3	GATA2	-0.314	T	0.543	D	NA	NA
	3	GATA2	0.347	D	0.782	D	NA	NA
	7	IKZF1	-0.707	T	0.606	D	NA	NA
	12	CDKN1B	-0.329	T	0.573	D	NA	NA
	19	TCF3	-0.236	T	0.728	D	NA	NA
	19	TCF3	0.436	D	0.855	D	NA	NA
	19	KEAP1	0.486	D	0.695	D	NA	NA
	19	JAK3	0.768	D	0.889	D	NA	NA
	19	JAK3	-0.019	T	0.549	D	NA	NA
	20	GNAS	0.228	D	0.675	D	NA	NA
MESO-163	1	RRAGC	0.34	D	0.588	D	NA	NA
	5	MAP3K1	0.435	D	0.597	D	NA	NA
	6	ROS1	0.108	D	0.609	D	NA	NA
	14	FOXA1	0.077	D	0.646	D	NA	NA
	14	DICER1	0.723	D	0.816	D	NA	NA
	17	TP53	0.964	D	0.993	D	Conflicting interpretations of pathogenicity	Conflicting interpretations of pathogenicity
	19	KEAP1	-0.261	T	0.512	D	NA	NA

Cells that have been cultured for multiple passages can show substantial drift of genetic and physiological characteristics that may confound pharmacogenomics and functional genomic studies.[9] To identify mutations that were due to serial long-term

passaging, early and late passage timepoint were compared for each cell culture. To focus on the driving mutations of cancer related genes, we used the gene list of the FDA approved platform for tumour profiling, MSK-IMPACT (*n*=468).[10] A limited proportion of non-synonymous and frameshift insertion mutations were detected. Hence, for the experimental assays, cells that had been cultured for less than 20 passages were used, as suggested by Pollard et al.[11] The table presents the predicted pathogenic mutations that were detected exclusively at the late passage MPM cell cultures. The pathogenicity prediction models are described elsewhere. [8]

LR=Logistic Regression, CLNSIG= Clinical Significance, CLNREVSTAT= Clinical Review Status, T=Tolerable, D=Deleterious

Supplementary Table 3

List of the 316 anticancer agents that were used for the high throughput drug screening assay.

Galiellalactone	Crizotinib
SR1 HCl	Vandetanib
VER 155008	Sotrastaurin
BAY 73-4506_Regorafenib	Panobinostat
RDEA119_Refametinib	ABT-199
Brivanib	AZD2014
GSK2126458	PKC412_Midostaurin
MGCD0103_Mocetinostat	AS703026_Pimasertib
BIBF 1120_Nintedanib	LY2228820 (CP868569)
FK 506_Tacrolimus	JNJ 26854165 (Serdemetan)
RD162	TAK-901
4-hydroxytamoxifen	AZ 3146
AVN944	2-methoxyestradiol (Panzem)
PF-04708671	Doxorubicin
AV-951 (Tivozanib)	EMD1214063
Camptothecin	NVP-BEZ235_Dactolisib
AZD1480	GSK2636771
Docetaxel	Irinotecan
MLN8237_Alisertib	INCB018424 (free base, Ruxolitinib)
Finasteride	AZD6244 (Selumetinib)
Clomifene citrate	Atorvastatin Ca
Idelalisib	S-trityl-L-cysteine, 40 mM
Tetramisole HCl	Prednisolone
Raloxifene	Aminolevulinic acid hydrochloride
1-methyl-D-tryptophan, 95%	Chloroquine diphosphate
Carmustine	Azacitidine
CUDC-101	Vismodegib
Cladribine	Trifluridine
Tubastatin A HCl	OSI-906_Linsitinib
Exemestane	Pentostatin
CHIR-258 (Dovitinib)	Tasocitinib_Tofacitinib
Mitomycin	Pipobroman
Nelarabine	17-DMAG (Alvespimycin)

Kanellakis NI, *et al. Thorax* 2020; 75:1004–1008. doi: 10.1136/thoraxjnl-2020-215027

Carboplatin	Sunitinib
(R)-Flurbiprofen (Tarenflurbil)	Stattic
Mitoxantrone	Imatinib
Allopurinol	Vatalanib
Thioguanine	Erismodegib
Dacarbazine	Fluorouracil
Altretamine	Vemurafenib
Ridaforolimus	Temozolomide
YM155	Ixazomib citrate
BIRB 796 (Doramapimod)	AG-014699_Rucaparib
PHA-739358 (Danusertib)	Canertinib
VX-11e	Tubacin
PCI-32765_Ibrutinib	PF-2341066 (Crizotinib)
ABT-263 (Navitoclax)	Homoharringtonine
CPI-613	Obatoclax Mesylate (GX15-070)
BI 2536	Nutlin-3
GSK 269962	BIIB021
MDV3100_Enzaluamide	TAK-733
Prednisone	PF670462
AZD8055	DCC-2036_Rebastinib
Enzastaurin	Idarubicin HCl
OSI-027	XL184_Cabozantinib
Rapamycin (sirolimus)	Simvastatin
MK-4827, HCl salt	MLN4924
HA-1077 (Fasudil)	CI-994_Tacedinaline
PIK-75 HCl	Dabrafenib Mesylate
Flutamide	Abitrexate/Methotrexate
Busulfan	NVP-AUY922
Cyclophosphamide	Vorinostat
Quinacrine HCl	Deferoxamine mesylate
Ifosfamide	Tamoxifen citrate
Aspirin (Acetylsalicylic Acid)	Methylprednisolone
Anastrozole	Temsirolimus
Iniparib (BSI-201, IND-71677)	AP24534 (Ponatinib)
Mitotane	Epirubicin hydrochloride
TGX-221	CAL-101
Oxaliplatin	Teniposide
ABT-751	Bosutinib

Methotrexate	Fulvestrant
PF4800567 hydrochloride	ABT-888 (Veliparib)
Pralatrexate	Triethylenemelamine
Tandutinib	Belinostat (PXD101)
Mercaptopurine	Osimertinib
Procarbazine hydrochloride	ZSTK474
Floxuridine	Bleomycin sulfate
Gemcitabine hydrochloride	Amifostine
Uracil mustard	Imiquimod
PX-866_Sonolisib	Streptozocin
I-BET151 (GSK1210151A)	Lapatinib
MK1775	PF 477736
Motesanib Diphosphate (AMG-706)	Lasofoxifene
Epothilone B (Patupilone)	Carfilzomib
LY2603618_Rabusertib	Crenolanib
AT9283	Toremifene citrate
ABT-869_Linifanib	Vincristine Sulfate (Oncovin)
RAF265	AT-406
AT 101	UCN-01
FK-866 HCl_Daporinad	(5Z)-7-Oxozeaenol
Estramustine sodium phosphate	CHR 2797_Tosedostat
AZD4547	GDC-0980
Bexarotene	PD-0332991
PF-04691502	MK-2206
Lapatinib, di-p-toluenesulfonate salt	Anagrelide
AC220_Quizartinib	BMS-911543
Dasatinib	Nilotinib
PLX4032_Vemurafenib	GSK1120212_Trametinib
Pilocarpine	Clafen (Cyclophosphamide, Endoxan)
Pemetrexed	ARRY-162_MEK-162
Letrozole	Gefitinib
Arsenic(III) oxide	Thio-TEPA
Clofarabine	Paclitaxel
Masitinib	Melphalan
Fludarabine phosphate	Melphalan hydrochloride
Bicalutamide	Tipifarnib (Zarnestra)
Erlotinib hydrochloride	Cobimetinib
Rofecoxib (Vioxx)	Dinaciclib (SCH727965)

Topotecan hydrochloride	Ceritinib
FG-4592	GDC-0941_Pictilisib
Pemetrexed, Disodium salt, Heptahydrate	Abiraterone
GSK 650394	Decitabine (Dacogen)
Mechlorethamine hydrochloride	Ixabepilone
XAV-939	Entinostat
Methoxsalen	Daunorubicin hydrochloride
Pomalidomide	Dactinomycin
Cytarabine hydrochloride	Chlorambucil
Megestrol acetate	Valrubicin
Tretinoin	Bendamustine hydrochloride
LY 333531 mesylate_Ruboxistaurin	Cabazitaxel
Lestaurtinib	AZD 7762 hydrochloride
Plerixafor	BIBW2992 (Tovok)_Afatinib
LY2784544_Gandotinib	BI 6727_Volasertib
Everolimus	MK-0752
KX2-391	R406_Tamatinib
XL880 (Foretinib)	BKM-120_Buparlisib
LY2157299	SB 743921
MGCD-265	Auranofin
PF 431396	JNJ-26481585_Quisinostat
Bimatoprost	Mithramycin A
Goserelin acetate	AZD1152-HQPA
Dacomitinib (monohydrate) (PF-00299804)	Perifosine aq/PBS
Cisplatin aq	GDC-0068
BMS-754807	Pazopanib
Axitinib	ARQ 197_Tivantinib
INK128	Sorafenib
Nilutamide	NVP-BGJ398
NVP-LDE225 (Diphosphate salt)	Dexamethasone (Decadron)
Metformin hydrochloride aq	XL-147
Pravastatin	Capecitabine
Zoledronic acid	Hydroxyurea
Valproic acid	Palbociclib
Enzalutamide	Aminoglutethimide
Olaparib	Romidepsin
Lomustine	PF-3845
CYT-387_Momelotinib	Plicamycin

Thalidomide	Varespladib
Roscovitine_Selicilib	Vinorelbine tartrate
Dexrazoxane	PAC-1
Amonafide	Alectinib
Lenalidomide	17-AAG (Tanespimycin, Geldanamycin)
Lomeguatrib	Omacetaxine mepesuccinate
Celecoxib	Prima-1 Met
Indibulin	Etoposide
Lenvatinib	Vinblastine sulfate
Bortezomib	Irinotecan hydrochloride
Pazopanib hydrochloride	Uridine triacetate

Kanellakis NI, *et al. Thorax* 2020; 75:1004–1008. doi: 10.1136/thoraxjnl-2020-215027

Supplementary Table 4

qPCR primers

Primer	Sequence (5'-3')	Length (nt)	Amplicon size (bp)
SSX2_F	GATGAAAGCCTCGGAGAAAA	20	230
SSX2_R	GCTTCTTGGGCATGATCTTC	20	
GAPDH_F	TGGAAGGACTCATGACCACA	20	163
GAPDH_R	TTCAGCTCAGGGATGACCTT	20	

F: Forward, R Reverse

Kanellakis NI, *et al. Thorax* 2020; 75:1004–1008. doi: 10.1136/thoraxjnl-2020-215027

Supplementary Table 5

Antibodies used for flow cytometry and intracellular staining

Antidody	Fluophore	ID	Company	RRID
CD107a	APC	560664	BD Pharmingen, Franklin Lakes, NJ	AB_1727417
HLA-A2	PE	558570	BD Pharmingen, Franklin Lakes, NJ	AB_647220
CFSE	488	C34554	Invitrogen Scientific, Waltham, MA	NA
7-AAD	Red	00-6993-50	Invitrogen Scientific, Waltham, MA	NA
IFNγ	AlexaFlour488	557718	BD Pharmingen, Franklin Lakes, NJ	AB_396827
TNFα	BV650	502912	BioLegend, San Diego, CA	AB_315264

NA = Not applicable

References

1. Johnson S, Chen H, Lo PK. In vitro Tumorsphere Formation Assays. *Bio Protoc* 2013;3(3)
2. Schmittgen TD, Livak KJ. Analyzing real-time PCR data by the comparative C(T) method. *Nat Protoc* 2008;3(6):1101-8.
3. Abd Hamid M, Wang RZ, Yao X, et al. Enriched HLA-E and CD94/NKG2A Interaction Limits Antitumor CD8(+) Tumor-Infiltrating T Lymphocyte Responses. *Cancer Immunol Res* 2019;7(8):1293-306. doi: 10.1158/2326-6066.CIR-18-0885
4. Van der Auwera GA, Carneiro MO, Hartl C, et al. From FastQ data to high confidence variant calls: the Genome Analysis Toolkit best practices pipeline. *Curr Protoc Bioinformatics* 2013;43:11 10 1-33. doi: 10.1002/0471250953.bi1110s43
5. Koboldt DC, Larson DE, Wilson RK. Using VarScan 2 for Germline Variant Calling and Somatic Mutation Detection. *Curr Protoc Bioinformatics* 2013;44:15 4 1-17. doi: 10.1002/0471250953.bi1504s44
6. McGowan SJ, Hughes JR, Han ZP, et al. MIG: Multi-Image Genome viewer. *Bioinformatics* 2013;29(19):2477-8. doi: 10.1093/bioinformatics/btt406
7. Landrum MJ, Lee JM, Benson M, et al. ClinVar: public archive of interpretations of clinically relevant variants. *Nucleic Acids Res* 2016;44(D1):D862-8. doi: 10.1093/nar/gkv1222
8. Dong C, Wei P, Jian X, et al. Comparison and integration of deleteriousness prediction methods for nonsynonymous SNVs in whole exome sequencing studies. *Hum Mol Genet* 2015;24(8):2125-37. doi: 10.1093/hmg/ddu733
9. Horvath P, Aulner N, Bickle M, et al. Screening out irrelevant cell-based models of disease. *Nat Rev Drug Discov* 2016;15(11):751-69. doi: 10.1038/nrd.2016.175
10. Cheng DT, Mitchell TN, Zehir A, et al. Memorial Sloan Kettering-Integrated Mutation Profiling of Actionable Cancer Targets (MSK-IMPACT): A Hybridization Capture-Based Next-Generation Sequencing Clinical Assay for Solid Tumor Molecular Oncology. *J Mol Diagn* 2015;17(3):251-64. doi: 10.1016/j.jmoldx.2014.12.006
11. Pollard SM, Yoshikawa K, Clarke ID, et al. Glioma stem cell lines expanded in adherent culture have tumor-specific phenotypes and are suitable for chemical and genetic screens. *Cell Stem Cell* 2009;4(6):568-80. doi: 10.1016/j.stem.2009.03.014